Three-Dimensional Structures of the Free and Antigen-Bound Fab from Monoclonal Antilysozyme Antibody HyHEL-63[†,‡]

Yili Li,[§,||,⊥] Hongmin Li,[§,⊥] Sandra J. Smith-Gill,[||] and Roy A. Mariuzza*[,§]

Center for Advanced Research in Biotechnology, University of Maryland Biotechnology Institute, 9600 Gudelsky Drive, Rockville, Maryland 20850, and National Cancer Institute, Frederick Cancer Research and Development Center, P.O. Box B, Frederick, Maryland 21702-1201

Received January 10, 2000; Revised Manuscript Received March 9, 2000

ABSTRACT: Antigen−antibody complexes provide useful models for studying the structure and energetics of protein−protein interactions. We report the cloning, bacterial expression, and crystallization of the antigen-binding fragment (Fab) of the anti-hen egg white lysozyme (HEL) antibody HyHEL-63 in both free and antigen-bound forms. The three-dimensional structure of Fab HyHEL-63 complexed with HEL was determined to 2.0 Å resolution, while the structure of the unbound antibody was determined in two crystal forms, to 1.8 and 2.1 Å resolution. In the complex, 19 HyHEL-63 residues from all six complementarity-determining regions (CDRs) of the antibody contact 21 HEL residues from three discontinuous polypeptide segments of the antigen. The interface also includes 11 bound water molecules, 3 of which are completely buried in the complex. Comparison of the structures of free and bound Fab HyHEL-63 reveals that several of the ordered water molecules in the free antibody-combining site are retained and that additional waters are added upon complex formation. The interface waters serve to increase shape and chemical complementarity by filling cavities between the interacting surfaces and by contributing to the hydrogen bonding network linking the antigen and antibody. Complementarity is further enhanced by small (<3 Å) movements in the polypeptide backbones of certain antibody CDR loops, by rearrangements of side chains in the interface, and by a slight shift in the relative orientation of the V_L and V_H domains. The combining site residues of complexed Fab HyHEL-63 exhibit reduced temperature factors compared with those of the free Fab, suggesting a loss in conformational entropy upon binding. To probe the relative contribution of individual antigen residues to complex stabilization, single alanine substitutions were introduced in the epitope of HEL recognized by HyHEL-63, and their effects on antibody affinity were measured using surface plasmon resonance. In agreement with the crystal structure, HEL residues at the center of the interface that are buried in the complex contribute most to the binding energetics ($\Delta G_{mutant} - \Delta G_{wild\ type} > 3.0$ kcal/mol), whereas the apparent contributions of solvent-accessible residues at the periphery are much less pronounced (<1.5 kcal/mol). In the latter case, the mutations may be partially compensated by local rearrangements in solvent structure that help preserve shape complementarity and the interface hydrogen bonding network.

Antibodies are versatile binding molecules developed by nature for the generation of a virtually unlimited repertoire of complementary molecular surfaces and, as such, constitute an excellent system for elucidating the principles governing protein−protein recognition (*1*). Antibody molecules are composed of light (L)[1] and heavy (H) polypeptide chains, each having variable (V) and constant (C) portions. The amino-terminal portions of the L and H chains (V_L and V_H, respectively) each contain three regions of highly variable length and sequence, the complementarity-determining regions (CDRs), which determine the conformation of the combining site and confer specific binding activity to the antibody molecule.

The three-dimensional structures of approximately 25 complexes between antibodies and various protein antigens have been determined in recent years, including hen egg white lysozyme (HEL) (*2*−*6*), influenza virus neuraminidase (*7*−*9*), horse cytochrome *c* (*10*), human tissue factor (*11*), *Escherichia coli* histidine phosphocarrier protein (*12*), staphylococcal nuclease (*13*), influenza virus hemagglutinin (*14*), human vascular endothelial growth factor (*15*), and antibodies bearing idiotypic determinants (*16*−*19*). These studies have permitted a detailed description of antigenic determinants and of antibody-combining sites. They have also provided important information on the general characteristics of protein−protein complexes, such as the size and chemical

[†] This work was supported by NIH Grant GM5280.

[‡] Atomic coordinates have been deposited in the Protein Data Bank as entries 1dqj, 1dqq, and 1dqm.

* To whom correspondence should be addressed. Telephone: (301) 738-6243. Fax: (301) 738-6255. E-mail: mariuzza@carb.nist.gov.

[§] University of Maryland Biotechnology Institute.

[||] Frederick Cancer Research and Development Center.

[⊥] These authors contributed equally to this work.

[1] Abbreviations: HEL, hen egg white lysozyme; PBS, phosphate-buffered saline; LB, Luria-Bertani medium; RU, resonance units; Fab, antigen-binding fragment; L chain, light chain; H chain, heavy chain; V region, variable region; C region, constant region; V_L, light chain variable region; V_H, heavy chain variable region; CDR, complementarity-determining region; FR, framework region.

10.1021/bi000054l CCC: $19.00
Published on Web 05/02/2000

nature of the interfaces and the mechanisms by which amino acid changes are accommodated. However, in only four cases (*6*, *10*, *11*, *20*) is the structure of the antibody in both free and antigen-bound forms known, too few to permit global generalizations concerning the molecular basis of antibody binding and specificity. Moreover, the relative contributions of surface complementarity, hydrophobicity, and hydrogen bonding to the energetics of binding, as well as the role of bound water molecules in complex stabilization, remain to be determined.

We have previously used the complex between the anti-HEL antibody D1.3 and its antigen (*20*) as a model for better understanding the underlying interactions that mediate protein−protein recognition (*21*−*23*). Alanine-scanning mutagenesis of D1.3 residues in contact with HEL in the crystal structure revealed that the energetics of binding to the antigen are dominated by a small subset (3 of 13) of contact residues (*21*, *23*), as described for the binding of growth hormone to its receptor (*24*). These findings are in marked contrast to those for the complex between D1.3 and the anti-D1.3 antibody E5.2 (*19*) in which most contact residues on both proteins mediate productive binding (*21*, *25*), such that complex stabilization is achieved by many productive interactions distributed over a large portion of the interface. Similar results have been reported for the barnase−barstar complex, in which nearly all residues within 4 Å of each other exhibit significant energetic coupling (*26*). The fact that different proteins employ different strategies for ligand binding highlights the complexity of protein−protein association reactions and serves as a warning against attempts to generalize them. It is therefore apparent that detailed structure−function studies of additional protein−protein complexes are required to arrive at a more comprehensive understanding of how structural features contribute to the affinity and specificity of binding reactions.

To this end, we have determined the high-resolution crystal structures of the antigen-binding fragment (Fab) of the anti-HEL antibody HyHEL-63 (*27*), both in the free form and complexed with its protein antigen. Although the structure of the closely related HyHEL-10 antibody bound to HEL has been reported (*4*), the structure of the HyHEL-10−HEL complex is only of moderate resolution (3 Å) and that of unbound HyHEL-10 is unknown. By permitting a detailed assessment of rerrangements in an antibody-combining site associated with complex formation, the structures of free and bound HyHEL-63 add to the limited database defining conformational changes in antibodies upon binding protein antigens. The HyHEL-63−HEL complex also reveals the extensive participation of both buried and exposed water molecules at the interface, linking the antigen and antibody and enhancing complementarity between their interacting surfaces. Interface waters were not observed in the HyHEL-10−HEL complex (*4*), presumably due to insufficient resolution. By individually mutating HEL residues in contact with HyHEL-63 and measuring the affinities of the mutants for the wild-type antibody using surface plasmon resonance, we identified two "hot spot" residues ($\Delta G_{mutant} - \Delta G_{wild\ type} > 3.0$ kcal/mol) for the HyHEL-63−HEL interaction. The effects of mutations in HEL on antibody binding are discussed in terms of the crystal structure of the HyHEL-63−HEL complex.

EXPERIMENTAL PROCEDURES

Cloning of the HyHEL-63 L and H Chains. Total mRNA was isolated from the HyHEL-63 hybridoma cell line (*27*) using a PolyATtract System 1000 mRNA purification kit (Promega, Madison, WI). First-strand cDNA synthesis was carried out with MMLV reverse transcriptase (Life Technologies, Gaithersburg, MD) using reverse primers for the κ L chain and IgG2a H chain (5′-ATCGGAGCTCTCAACACTCATTCCTGTTGAAGCTCTT-3′ and 5′-ATCGAAGCTTTCAAATTTTCTTGTCCACCTTGGTGCT-3′, respectively). The cDNAs were used for PCR amplification of the L chain with the κ reverse primer and a forward primer (5′-ATCGAAGCTTTGGATTTCAGCCTCCAG-3′) complementary to the HyHEL-10 Vκ leader sequence (*28*). Similarly, the H chain was amplified using the IgG2a reverse primer and a forward primer (5′-TGTACCTGTTGACAAGCCTTCCGG-3′) complementary to the HyHEL-10 V_H leader sequence (*28*). The PCR products were subjected to direct sequencing using a *fmol* DNA Cycle Sequencing System (Promega). The nucleotide and deduced amino acid sequences of the V_L and V_H regions of HyHEL-63 are shown in Figure 1, aligned with those of HyHEL-10.

Production of Fab HyHEL-63 by in Vitro Refolding. DNA fragments encoding the V_L and C_L domains of the L chain and the V_H and C_H1 domains of the H chain were generated by PCR and restricted with *Nde*I−*Sac*I and *Nde*I−*Hin*dIII, respectively, for independent insertion into expression vector pET22b (Novagen, Madison, WI). The sequences of both constructs were verified using a DNA Cycle Sequencing Kit (Promega). For protein production, *Escherichia coli* BL21-(DE3) cells were separately transformed with the pET22b-L chain and pET22b-H chain plasmids. Precultures (3 mL) were grown at 37 °C overnight in Luria-Bertani medium (LB) containing 60 μg/mL ampicillin. These precultures were then used to inoculate 500 mL of LB with the same antibiotic concentration. The bacteria were grown at 37 °C to an absorbance of 0.6−0.8 at 600 nm, and isopropyl β-D-thiogalactoside was added to a final concentration of 1 mM. After further incubation for 3 h, the bacteria were harvested by centrifugation and frozen at −70 °C until they were used.

For refolding Fab HyHEL-63, the cell pellets were resuspended in $^1/_{10}$ culture volume of 50 mM Tris-HCl (pH 8.0) containing 2 mM EDTA, 100 μg/mL lysozyme, and 1% (v/v) Triton X-100. After 30 min at room temperature, the suspensions were sonicated with a microtip and centrifuged at 10000*g* for 15 min at 4 °C. The supernatants were discarded and the pellets washed three times with 50 mM Tris-HCl (pH 8.0), 2 mM EDTA, and 1% (v/v) Triton X-100 and once with 50 mM Tris-HCl (pH 8.0) and 2 mM EDTA. Inclusion bodies were solubilized by overnight incubation at room temperature in 0.1 M Tris-HCl (pH 8.5), 6 M guanidine-HCl, 2 mM EDTA, and 0.1 M DTT at a protein concentration of 2 mg/mL. The solubilized L and H chains were mixed in a 1:1 molar ratio and diluted 33-fold into 0.1 M Tris-HCl (pH 8.5) containing 2 mM EDTA, 4 mM oxidized glutathione, and 0.4 M L-arginine. The Fab fragment was left to refold at 4 °C for at least 96 h.

To purify correctly folded Fab HyHEL-63, the renaturation mixture was applied directly to an HEL affinity column (UltraLink Biosupport Medium, Pierce, Rockford, IL) pre-equilibrated with phosphate-buffered saline (PBS). The

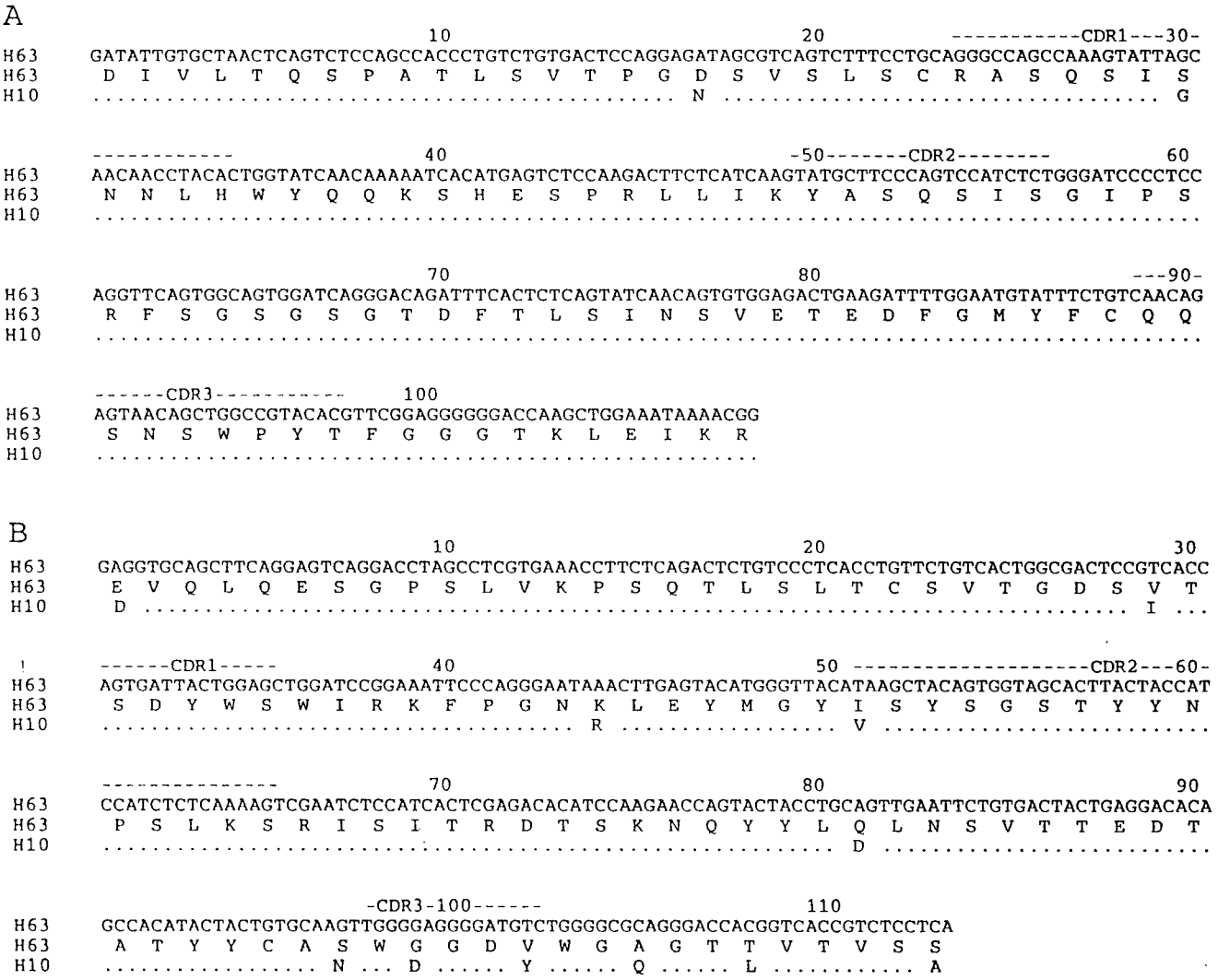

FIGURE 1: (A) Nucleotide and deduced amino acid sequences of the V_L region of HyHEL-63 (designated H63). (B) Nucleotide and deduced amino acid sequences of the V_H region of HyHEL-63. The amino acid sequence of HyHEL-10 (designated H10) (*28*) is represented in panels A and B only at positions where it differs from that of HyHEL-63. CDR boundaries are defined as described previously *59*.

column was washed with 10 volumes of 0.1 M Tris-HCl (pH 8.0) containing 1 M NaCl, followed by 5 volumes of PBS. Bound protein was eluted with 50 mM glycine-HCl (pH 2.5). Fractions were immediately neutralized with 1.0 M Tris-HCl (pH 8.0), and those containing Fab HyHEL-63 were pooled and dialyzed overnight against 50 mM Tris-HCl (pH 8.5). Further purification was carried out on a Mono Q anion exchange FPLC column (Pharmacia, Uppsala, Sweden) equilibrated with the same buffer and developed with a linear NaCl gradient. Recombinant Fab HyHEL-63 eluted as two major peaks between 0.06 and 0.08 M NaCl, both of which had HEL-binding activity. Although Fab from both peaks crystallized, the material in the first peak yielded consistently better results and was therefore used for all subsequent studies.

Crystallization and Data Collection. Initial crystallization conditions for the free and HEL-complexed Fab HyHEL-63 were established using the broad screening method of Jancarik and Kim (*29*) with a Hampton Crystal Screen Kit (Hampton Research, Laguna Niguel, CA). A number of conditions gave crystals for both free and complexed Fab. Bar-shaped crystals of free Fab HyHEL-63, with dimensions up to 0.15 mm × 0.15 mm × 0.5 mm, were obtained at room temperature in hanging drops by mixing 1 μL of a protein solution at a concentration of 10 mg/mL with an equal volume of reservoir solution containing 16% (w/v) PEG 8000, 0.1 M KH_2PO_4, and 0.1 M Tris-HCl (pH 7.5). For the complex, HEL and Fab HyHEL-63 were mixed in an equimolar ratio at a concentration of 10 mg/mL. The complexed Fab crystallized at room temperature in hanging drops containing 15% (w/v) PEG 4000, 0.1 M ammonium acetate, and 0.05 M sodium acetate (pH 4.6). The crystals grew as large plates, measuring up to 0.4 mm × 0.4 mm × 0.1 mm.

X-ray diffraction data from crystals of both free Fab HyHEL-63 and the Fab HyHEL-63−HEL complex were measured at 100 K using an in-house 345 mm MarResearch Image Plate detector. The crystals were washed several times with mother liquor and then transferred to a cryoprotectant solution (mother liquor containing 25% glycerol), prior to flash-cooling in a nitrogen stream. Although the shapes of the free Fab crystals used for data collection were the same, two sets of diffraction data yielded two different crystal forms with space groups *C*2 and *P*1 (Table 1), possibly due to slight differences on flash-cooling. All sets of diffraction data were processed and scaled using DENZO/SCALEPACK (*30*), followed by data reduction using programs from the CCP4 suite (*31*). Data collection statistics are summarized in Table 1.

Table 1: Crystal Data and Structure Refinement Statistics

	H63-P1	H63-C2	H63-HEL
	Data Collection		
space group	*P*1	*C*2	$P4_22_12$
unit cell dimensions (Å)	$a = 39.94$, $b = 67.34$, $c = 84.39$, $\alpha = 81.52°$, $\beta = 77.04°$, $\gamma = 87.6°$	$a = 162.36$, $b = 39.74$, $c = 70.29$, $\beta = 98.1°$	$a = b = 90.58$, $c = 150.06$
asymmetric unit	2 Fab H63	1 Fab H63	1 Fab H63-HEL
resolution (Å)	1.8	2.1	2.0
no. of observations	145275	88367	366760
no. of unique reflections	68027	26702	45762
completeness (%)	86.5 (54.5)[a]	94.0 (67.3)[a]	92.7 (85.0)[a]
mean $I/\sigma(I)$	16.0 (2.0)[a]	12.8 (1.7)[a]	19.6 (5.1)[a]
R_{sym} (%)[b]	4.9 (31.5)[a]	9.0 (32.8)[a]	8.9 (37.1)[a]
	Refinement		
resolution range (Å)	100−1.8	100−2.1	100−2.0
R_{work} (%)[b]	21.0	22.5	21.7
R_{free} (%)[b]	25.5	26.9	24.9
no. of non-hydrogen protein atoms	6488	3235	4245
no. of water molecules	858	336	467
average *B* factors for atoms (Å^2)			
overall	26.7	30.5	25.5
V domain	27.1/20.8	36.2	21.3
C domain	28.6/25.5	23.1	24.4
lysozyme			30.9
water	35.2	35.4	33.6
rms deviations from ideality			
bonds (Å)	0.005	0.006	0.005
angles (deg)	1.4	1.373	1.4
dihedrals (deg)	27.1	27.5	26.3
improper dihedrals (deg)	0.80	0.83	0.77
Ramachandran plot outliers	Ala51L/Ala51L	Ala51L	Ala51L

[a] Values in parentheses correspond to the highest-resolution shell (1.9−1.8 Å for H63-P1, 2.2−2.1 Å for H63-C2, and 2.1−2.0 Å for H63-HEL). [b] $R_{sym} = \Sigma|I_j - \langle I\rangle|/\Sigma I_j$, where I_j is the intensity of an individual reflection and $\langle I\rangle$ is the average intensity of that reflection. R_{work} (R_{free}) $= \Sigma||F_o| - |F_c||/\Sigma|F_o|$, where F_c is the calculated structure factor; 5% of data for H63-P1 and H63-HEL were used for R_{free} and 10% for H63-C2.

Structure Determination and Refinement. The structure of free Fab HyHEL-63 in space group *C*2 (designated H63-C2) was determined by the molecular replacement method with the program AMoRe (*32*). Before the structure determination, sequence homology searches of antibodies with known three-dimensional structures in the Protein Data Bank (PDB) were performed using the on-line program MPsrch with a Smith-Waterman dynamic algorithm (http://www.dna.affrc.go.jp/htdocs/MPsrch/index.html) (*33*). High-resolution structures whose sequences are very homologous to HyHEL-63 were chosen as search models. The variable (V_L and V_H) and constant (C_L and C_H) modules were treated as two separate search models in molecular replacement calculations, to account for any relative positional variability between the V and C modules of Fabs. A V_L and V_H search module was composed of the V_L domain of Fab OPG2 (2.0 Å resolution, PDB entry 1OPG, 96.4% degree of sequence homology to V_L of HyHEL-63) (*34*) and the V_H domain of Fab 184.1 (1.95 Å resolution, PDB entry 1OSP, 85.7% degree of sequence homology to V_H of HyHEL-63) (*35*). The model was constructed by superposition of the V_L domain of OPG2 Fab onto that of Fab184.1. A search module for C_L and C_H was taken from the atomic coordinates of the 1.9 Å resolution structure of the Fab of the IgG2a antibody D2.3 (PDB entry 1YEC, 100% homology) (*36*). These two search models were subjected to rotational and translational function calculations. The solution for C_L and C_H was found first. The fixed C module was then used to place V_L and V_H with the phased translation function calculation. Rigid-body refinement of the correct V and C module solutions gave a correlation coefficient of 54.5% and an R_{factor} of 40.9% at 10−4 Å resolution. Refinement was carried out using X-PLOR3.1 (*37*) and CNS0.4 (*38*), including rigid-body refinement, iterative cycles of simulated annealing, positional refinement, torsion angle refinement, and temperature factor (*B*) refinement, interspersed with model rebuilding into σ_A-weighted $F_o - F_c$ and $2F_o - F_c$ electron density maps using TURBO-FRODO (*39*). Solvent molecules were gradually added to the model; only those maintaining acceptable bonding distances and *B* factors of less than 60 Å^2 were retained in the final model. Bulk solvent correction and initial anisotropic *B* factor scaling were applied to the X-ray data. The final Fab H63-C2 structure determined to 2.1 Å resolution has an R_{factor} of 22.5% and an R_{free} of 26.9%; the model includes 336 water molecules (Table 1).

The V and C modules of the partially refined Fab H63-C2 structure were used as search models for structure determinations of Fab HyHEL-63 in the *P*1 space group (designated H63-P1) and the Fab HyHEL-63−HEL complex with AMoRe (*32*). The search model for HEL was taken from the coordinates of the Fv D1.3−HEL D18A mutant complex (1.5 Å resolution, PDB entry 1A2Y) (*23*). Similar protocols for molecular replacement as described above were used here. The results from the rotation function calculations, independently determined for each of the models, were applied in the translation function calculations, first for the V module, then for the C module, and finally for HEL in the case of the complex. Clear solutions were obtained in each case. Iterative cycles of refinement using X-PLOR3.1 (*37*) and CNS0.4 (*38*) followed by manual model building resulted in final R_{factor} values of 21.0% for Fab H63-P1 at 1.8 Å resolution and of 21.7% for the Fab HyHEL-63−HEL complex at 2.0 Å resolution. Summaries of the structure refinement statistics are given in Table 1.

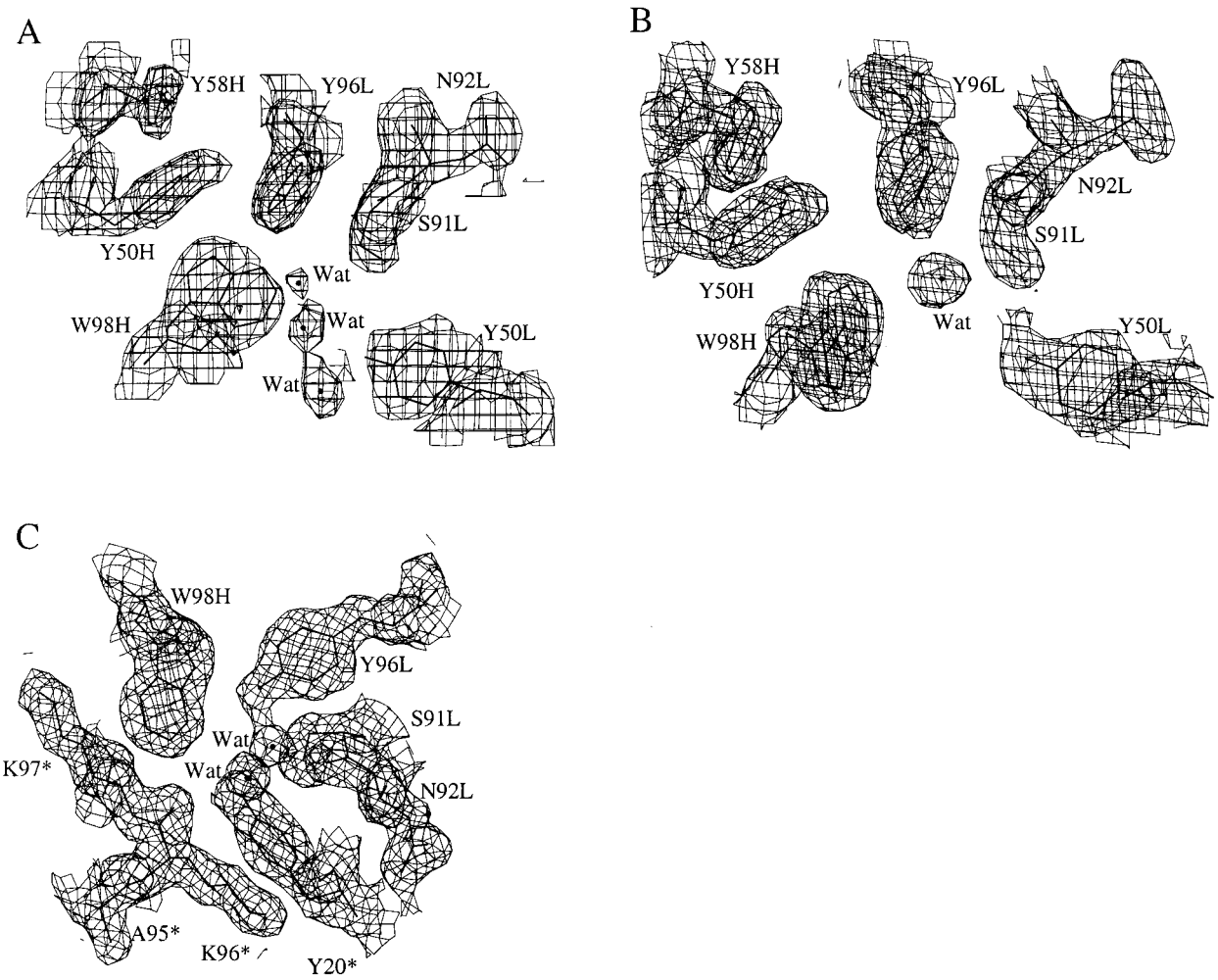

FIGURE 2: (A) Electron density from the final 2.1 Å $2F_o - F_c$ map of free Fab H63-C2 in the region of the combining site, showing bound water molecules (Wat). Contours are at 1σ. (B) Electron density from the final 1.8 Å $2F_o - F_c$ map, contoured at 1σ, of free Fab H63-P1 (molecule 1) in the region of the combining site. (C) Electron density from the final 2.0 Å $2F_o - F_c$ map of the Fab HyHEL-63−HEL complex in the region of the interface. HEL residues are indicated with asterisks. Contours are at 1σ.

Accessible surface areas were calculated by X-PLOR3.1 (*37*) with the algorithm of Lee and Richards (*40*) using a probe radius of 1.7 Å. Molecules were aligned in three dimensions using the program ALIGN (*41*). Hydrogen bonds were assigned with the program CONTACT from the CCP4 suite (*31*) using a cutoff distance of 3.4 Å.

Production of HEL Mutants. HEL mutants were produced using an Invitrogen *Pichia* Expression Kit (San Diego, CA). A cDNA sequence encoding the wild-type protein fused with the leader sequence of α mating factor was cloned into plasmid pPic9 as a *Xho*I−*Not*I fragment (*43*); mutagenesis was carried out by PCR. Yeast from a single colony transformed with this plasmid was grown in 25 mL of BMGY medium at 28−30 °C in a shaking incubator at 200−250 rpm. After the culture reached an absorbance of 2.0 at 600 nm, the cells were harvested by centrifugation at 1500*g* for 5 min at room temperature. The pellet was suspended in BMMY medium to an absorbance of 1.0 prior to induction. Methanol was added to the culture to a final concentration of 0.5% (v/v) every 24 h to maintain induction. The culture was harvested by centrifugation after 3 days. The supernatant containing the secreted HEL mutant protein was dialyzed overnight against 0.1 M ammonium acetate (pH 9.0) and loaded on a 3 mL CM-Sepharose Fast Flow column (Pharmacia) previously equilibrated with the same buffer (*44*). The column was washed with 10 volumes of buffer; the mutant was eluted with 5 column volumes of 0.5 M ammonium acetate (pH 9.0). Further purification was carried out on a Mono S cation exchange FPLC column (Pharmacia) equilibrated with 50 mM MES (pH 6.5) and developed with a linear NaCl gradient. All mutants eluted between 0.2 and 0.4 M NaCl.

Affinity Measurements. The interaction of soluble Fab HyHEL-63 with immobilized wild-type HEL and HEL mutants was assessed by surface plasmon resonance detection using a BIAcore 1000 instrument (Pharmacia Biosensor, Uppsala, Sweden) as described previously (*21*, *23*). The data were analyzed using the BIAevaluation 2.1 software package (Pharmacia). Association constants (K_A values) were determined from Scatchard analysis, after correction for nonspecific binding, by measuring the concentration of free reactants and the complex at equilibrium. Standard deviations for two or more independent K_A determinations were typically <20%.

RESULTS AND DISCUSSION

Quality of the Structures. The electron density maps for all three structures (free Fab HyHEL-63 in two crystal forms and the FabHyHEL-63−HEL complex) are of high quality, as shown in Figure 2. There are no main chain breaks in

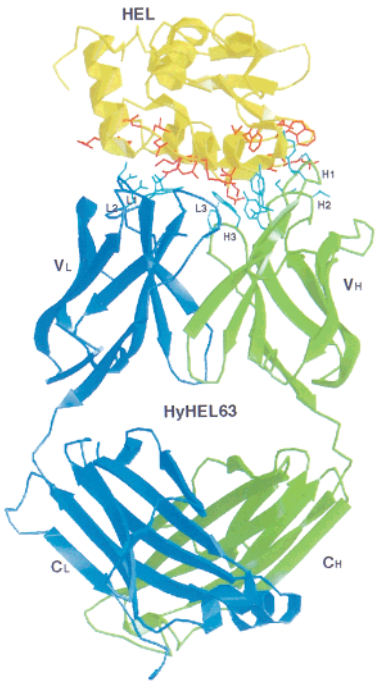

FIGURE 3: Ribbon diagram of the Fab HyHEL-63−HEL complex. Colors are as follows: HEL (yellow), L chain (blue), and H chain (green). Residues of HEL and HyHEL-63 involved in interactions in the antigen−antibody interface are red and blue, respectively. CDRs 1−3 of the V_L and V_H domains are numbered.

electron density in any of the structures, except for that of free Fab HyHEL-63 in space group *C*2 (H63-C2), in which poor density was observed for a loop in the C_L domain composed of residues 128−131. This loop, which is associated with the interdomain disulfide bridge between C_L residue Cys128 and C_H C-terminal residue Cys214, has different main chain conformations in the three structures. As differences are also observed in other IgG2a Fab structures (*36*, *45*), the loop of residues 128−131 is apparently highly flexible. No electron density was observed for the side chains of six, eight, and four residues of free H63-C2, Fab HyHEL-63 in space group *P*1 (H63-P1), and the HyHEL-63−HEL complex, respectively. None of these residues is located in the antigen-combining site. In all three cases, V_L CDR2 Ala51, clearly defined in the electron density, is an outlier in the Ramachandran plot; this residue corresponds to the second residue ($i + 1$) of a γ turn, which is frequently observed to exhibit unusual main chain torsion angles in antibody structures (*6*, *10*). In the HyHEL-63−HEL complex, V_L CDR1 Ser30 is also located in a disallowed region of the Ramachandran plot. This residue is at the second position of a II′ type β turn, which is generally occupied by glycine. The errors in atomic coordinates are 0.24 Å for the free Fab H63-P1, 0.27 Å for the free Fab H63-C2, and 0.25 Å for the HyHEL-63−HEL complex, as estimated by the method of Luzzatti (*46*). These estimates appear reasonable, as the errors increase with decreasing resolution.

Antigen−Antibody Interactions. Figure 3 shows a ribbon diagram of the Fab HyHEL-63−HEL complex. The HEL epitope recognized by HyHEL-63 is composed of 21 residues from three separate polypeptide segments of the antigen that form a contiguous patch on its surface: (1) Arg14, His15, Gly16, Asp18, Asn19, Tyr20, and Arg21; (2) Trp62, Trp63, Arg73, Leu75, and Asn77; and (3) Thr89, Asn93, Lys96, Lys97, Ile98, Ser100, Asp101, Gly102, and Asn103. Residues Thr89, Asn93, Lys96, Lys97, and Ile98 are on the exposed face of an α-helix that is oriented diagonally across the antibody-combining site with its N-terminus contacting V_L CDR2 and its C-terminus contacting V_H CDR1 and V_H CDR2 (Figure 2). This epitope is very similar to that recognized by HyHEL-10 (*4*), as expected from the fact that the V_L and V_H sequences of HyHEL-63 differ from those of HyHEL-10 at only 13 positions (Figure 1). All six CDRs of the variable domains of HyHEL-63 are involved in contacts with HEL. Nine L chain CDR residues, 10 H chain CDR residues, and 1 H chain framework region (FR) residue contribute to the contacts: Ser30, Asn31, and Asn32 (V_L CDR1); Tyr50 and Gln53 (V_L CDR2); Ser91, Asn92, Trp94, and Tyr96 (V_L CDR3); Thr30 (V_H FR1); Ser31, Asp32, and Tyr33 (V_H CDR1); Tyr50, Ser52, Tyr53, Ser54, Ser56, and Tyr58 (V_H CDR2); and Trp98 (V_H CDR3).

Table 2: Interface Hydrogen Bonds in the HyHEL-63−HEL and HyHEL-10−HEL Complexes[a]

HyHEL-63	distance (Å)	HEL	distance (Å)	HyHEL-10
V_L Asn31 Oδ1	3.01	Lys96 Nζ	2.74	V_L Asn31 Oδ1
Nδ2	3.21	His15 O		
V_L Asn32 Oδ1	2.80	Lys96 Nζ		
Nδ2	3.20	Gly16 O	3.24	V_L Asn32 Nδ2
V_L Gln53 Oε1	3.30	Asn93 Oδ1	2.60	V_L Gln53 Oε1
Nε2	2.84	Asn93 Oδ1	3.29	Nε2
		Tyr20 OH	3.39	V_L Ser91 O
V_L Asn92 O	2.81	Arg21 N	3.26	V_L Asn92 O
Nδ2	3.27	Asn19 O		
V_L Tyr96 OH	3.28	Arg21 NH1	2.89	V_L Tyr96 OH
V_H Thr30 O	3.30	Arg73 Nε	3.06	V_L Thr30 O
O	2.47	Arg73 NH2		
		Arg73 NH1	2.46	V_H Ser31 Oγ
V_H Asp32 Oδ2[b]	2.67	Lys97 Nζ	3.61	V_H Asp32 Oδ2[b]
V_H Tyr33 OH	2.64	Lys97 O	3.00	V_H Tyr33 OH
		Ile98 O	3.17	OH
V_H Tyr50 OH	3.05	Arg21 NH1	2.51	V_H Tyr50 OH
OH	3.39	Arg21 NH2	2.61	
OH	2.60	Ser100 O		
		Lys97 O	3.00	OH
V_H Ser52 Oγ	2.70	Asp101 Oδ1		
V_H Tyr53 OH	3.18	Asn103 Oδ1		
		Asp101 Oδ1	2.31	
V_H Tyr53 OH		Asp101 Oδ2	2.99	OH
V_H Ser54 N	3.14	Asp101 Oδ1		
Oγ	2.49	Asp101 Oδ1		
Oγ	2.93	Asp101 Oδ2		
V_H Ser56 Oγ	3.22	Asp101 Oδ1		
Oγ	2.82	Gly102 N	3.34	V_H Ser56 Oγ
		Asp101 O	3.38	Oγ
V_H Tyr58 OH	3.38	Asp101 O		
		Gly102 N	2.55	V_H Tyr58 OH

[a] Atomic coordinates for the HyHEL-10−HEL complex (*4*) are from the Protein Data Bank. [b] Salt bridge.

The interactions between HyHEL-63 and HEL include extensive van der Waals contacts and hydrogen bonds, as well as one salt bridge (V_H Asp32 Oδ2−HEL Lys97 Nζ). In addition to 24 hydrogen bonds (including the salt bridge) (Table 2), there are 170 van der Waals contacts in the interface (Table 3). The total buried surface area upon complex formation is 1901 Å^2, of which 917 Å^2 is contributed by the antibody and 984 Å^2 by HEL (Table 3). Of the 20 contacting residues of HyHEL-63, 8 are aromatic (Table 3). Four of the 8 aromatic residues (V_L CDR2 Tyr50, V_L CDR3 Tyr96, V_H CDR1 Tyr33, and V_H CDR2 Tyr50) are completely or predominantly (>90%) buried in the interface. These residues form a hydrophobic cluster centered about

Table 3: Buried Surface Areas and van der Waals Contacts for the HyHEL-63−HEL and HyHEL-10−HEL Complexes[a]

residue number		buried surface area (Å^2)		no. of contacts		residue number		buried surface area (Å^2)		no. of contacts	
H63/H10		H63	H10	H63	H10	HEL		H63	H10	H63	H10
27L1	Gln	6	−	−	−	13	Lys	1	4	−	−
28L1	Ser	8	1	−	−	14	Arg	22	23	1	1
30L1	Ser/Gly	47	24	3	5	15	His	16	15	7	7
31L1	Asn	51	57	16	20	16	Gly	32	42	8	14
32L1	Asn	28	29	10	4	18	Asp	17	10	1	−
						19	Asn	40	16	3	1
49L2	Lys	13	4	−	−	20	Tyr	63	70	11	10
50L2	Tyr	46	60	9	15	21	Arg	131	136	17	21
53L2	Gln	58	60	10	9	22	Gly	2	−	−	−
						62	Trp	26	21	1	−
67L	Ser	7	13	−	−	63	Trp	20	17	5	4
						73	Arg	92	78	11	18
91L3	Ser	15	14	3	5	75	Leu	47	64	5	2
92L3	Asn	67	69	10	8	77	Asn	37	27	2	−
93L3	Ser	14	6	−	−	89	Thr	25	17	3	2
94L3	Trp	14	13	3	2	93	Asn	69	51	10	12
96L3	Tyr	10	14	2	4	96	Lys	37	53	13	15
total		384	364	66	72						
						97	Lys	93	84	17	8
						98	Ile	−	−	3	3
27H	Asp	8	2	−	−	99	Val	1	1	−	−
28H	Ser	−	1	−	−	100	Ser	44	38	10	10
30H	Thr	37	54	7	13	101	Asp	74	94	33	34
31H1	Ser	64	42	7	7	102	Gly	50	36	6	6
32H1	Asp	43	42	5	1	103	Asn	30	22	3	−
33H1	Tyr	68	71	12	12	104	Gly	1	−	−	−
						107	Ala	5	7	−	−
50H2	Tyr	17	13	9	11	111	Trp	−	1	−	−
52H2	Ser	5	6	8	5	119	Asp	1	−	−	−
53H2	Tyr	129	109	21	22	128	Arg	−	1	−	−
54H2	Ser	21	12	8	2	129	Leu	1	−	−	−
56H2	Ser	20	23	7	7	total		984	928	170	168
58H2	Tyr	52	52	9	12						
98H3	Trp	60	52	11	4						
99H3	Gly	8	−		−						
101H3	Asp	5	9	−	−						
102H3	Val/Tyr	−	7	−	−						
total		917	859	170	168						

[a] van der Waals contacts of <4.0 Å. L1−L3 refer to V_L CDR1, V_L CDR2, and V_L CDR3, respectively; H1−H3 refer to V_H CDR1, V_H CDR2, and V_H CDR3, respectively.

another aromatic residue, V_H CDR3 Trp98. Although V_H Trp98 is only 73% buried upon complex formation, it contributes 60 Å^2 to the buried surface area and makes 11 van der Waals contacts with HEL. Residue V_H CDR2 Tyr53, at the periphery of the interface, is 79% buried and penetrates into a cleft of the antigen, interacting with HEL residues Trp62, Trp63, Leu75, Asp101, and Asn103 (Table 2). Two other aromatic residues (V_L CDR3 Trp94 and V_H CDR2 Tyr58) are less buried (21 and 49%, respectively) and are situated around the hydrophobic core. Thus, the interacting surface of HyHEL-63 is mainly hydrophobic (Figure 4A), as observed in other antigen−antibody complexes (*2*−*19*).

In contrast to the contacting surface of the antibody, hydrophilic residues predominate on the HEL side of the interface. Of the 21 residues of the antigen in contact with HyHEL-63, only 5 are hydrophobic, including 3 aromatic residues (Tyr20, Trp62, and Trp63). Of the three aromatic residues, Tyr20 is completely buried in the interface and points toward the hydrophobic cluster at the antibody-combining site. HEL residues Trp62 and Trp63 are only partially buried (23 and 54%, respectively) and form the base of the catalytic cleft which accommodates V_H Tyr53 in the complex. Of the 16 hydrophilic residues, 7 are charged (Arg14, Asp18, Arg21, Arg73, Lys96, Lys97, and Asp101),

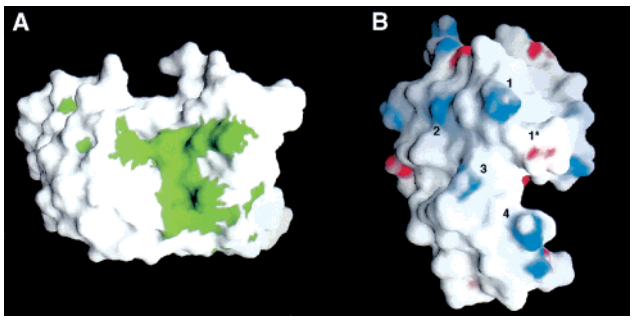

FIGURE 4: (A) Molecular surface of Fab HyHEL-63 viewed at the side that interacts with HEL in the Fab HyHEL-63−HEL complex drawn using GRASP (*60*). Green denotes hydrophobic regions. (B) Molecular surface of HEL that interacts with Fab HyHEL-63. Blue denotes regions of positive potential and red regions of negative potential. The two proteins are oriented such that they may be docked by folding the page along a vertical axis between them. HEL residues Arg21, Lys96, Lys97, Arg73, and Asp101 are labeled 1−4 and 1*, respectively.

5 of them positively. However, the charged side chains are mostly located at the periphery of the HEL binding surface and tend to point away from the center of the interface, resulting in a rather neutral binding surface (Figure 4B). This surface interacts with the aromatic cluster of the antibody.

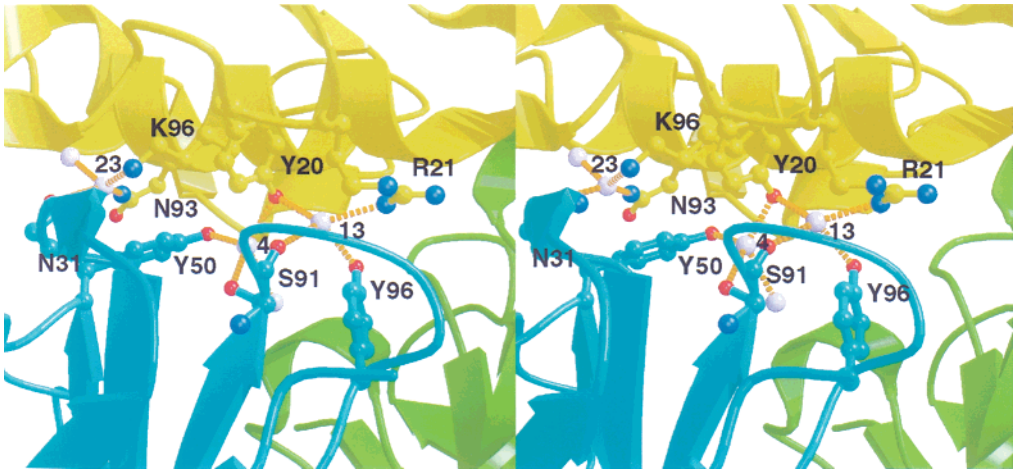

FIGURE 5: Stereodiagram of the Fab HyHEL-63−HEL interface showing bound water molecules. Colors are as follows: HEL (yellow), L chain (blue), and H chain (green). Interface waters are drawn as pink spheres. Waters 4, 13, and 23 are completely buried in the complex (see the text). Nitrogen and oxygen atoms are colored blue and red, respectively. Hydrogen bonds are represented as dotted orange lines.

The side chains of HEL residues Lys96 and Lys97 intercalate between antibody residues V_L Tyr50, V_H Tyr33, and V_H Trp98. In the complex, Lys97 is neutralized by forming a salt bridge with V_H Asp32, the only charged residue found in the antibody-combining site; Lys96 is neutralized by hydrogen bonding to V_L Asn31 and V_L Asn32 (Table 2). Although HEL residues Arg21 and Arg73 are only partially buried (80 and 68%, respectively), they contribute 13% (131 Å^2) and 10% (92 Å^2), respectively, of the total buried surface area of the antigen (Table 3). The HEL Arg21 side chain is stabilized by hydrogen bonds to the hydroxy groups of V_L Tyr96 and V_H Tyr50 and to two water molecules (see below), while Arg73 makes hydrogen bonds to the main chain carbonyl group of V_H Thr30. The negative charge of HEL Asp101 is partially neutralized by the Nδ2 group of HEL Asn103. In the complex, HEL Asp101 is completely buried and forms six hydrogen bonds with V_H residues Ser52, Ser54, Ser56, and Tyr58 (Table 2). The other two charged HEL residues (Arg14 and Asp18) are less buried (<20%).

Water Interactions at the Interface. The interacting surfaces of HyHEL-63 and HEL have a shape correlation statistic (Sc) of 0.70, slightly higher than the observed mean Sc value of 0.64−0.68 for antigen−antibody interfaces (*47*), indicating somewhat better shape complementarity. Gaps in the HyHEL-63−HEL interface are generally filled with trapped water molecules, as observed in other high-resolution antigen−antibody structures (*10*, *11*, *19*, *20*). In particular, the surface defined by V_L residues Ser91 and Tyr96 and V_H residues Trp98 and Tyr50 is up to 1.6 Å away from the surface defined by HEL residues Tyr20, Arg21, Lys96, Lys97, and Ser100, creating a large cavity. Three water molecules (designated as Wat4, Wat13, and Wat23) are completely buried between these two surfaces, filling the cavity and enhancing surface complementarity (Figure 5). Interestingly, one of these waters (Wat4) is present in both free Fab HyHEL-63 structures (H63-C2 and H63-P1), as well as in a triclinic HEL structure (PDB entry 2LZT) (*48*); in contrast, Wat13 is present in the triclinic HEL structure but not in either of the free Fab structures. Wat4 makes two hydrogen bonds to V_L residues Tyr50 and Ser91 and one hydrogen bond to HEL residue Tyr20, as well as to a water molecule (Table 4). Wat13 bridges V_L residues Ser91 and Tyr96 and HEL residues Tyr20 and Arg21. Wat23 is only present in the HyHEL-63−HEL complex, making hydrogen bonds to V_L Asn31 Oδ1 and to Asn23 Nδ2 and Lys96 Nζ of HEL. In addition to these 3 buried water molecules, 8 more waters (Wat15, Wat51, Wat58, Wat79, Wat121, Wat174, Wat359, and Wat418) interact directly with both Fab HyHEl-63 and HEL (Table 4); however, these are exposed to solvent. Six of them are not found in either of the free Fab HyHEL-63 structures. Two (Wat51 and Wat79) are found in the free H63-C2 structure, but not in the H63-P1 structure. Of the 11 interface water molecules listed in Table 4, 2 (Wat58 and Wat79) are conserved in both triclinic (*48*) and tetragonal HEL (PDB entry 1HEL) (*49*), 2 (Wat4 and Wat13) are present in triclinic HEL only, and 1 (Wat21) is found in a monoclinic HEL structure (PDB entry 1LMA) (*50*). Therefore, 6 of the 11 interface waters are present in at least one of the free antibody and/or antigen structures. The 5 remaining waters, including a buried one (Wat23), are absent in the structures of free HyHEL-63 and HEL and therefore appear to be trapped upon complex formation. Surprisingly, of the 11 interface solvent molecules, only 1

Table 4: Hydrogen Bonds Made by Water Molecules in the HyHEL-63−HEL Interface

H63/water	water[a]	HEL/water
V_L Tyr50 Oη	Wat4	Tyr20 Oη
V_L Ser91 Oγ	Wat4	Wat69
V_L Ser91 O	Wat13	Tyr20 Oη
V_L Tyr96 Oη	Wat13	Arg21 Nη1
V_L Gln53 Oϵ1	Wat15	Thr89 O
	Wat15	Wat23
V_L Asn31 Oδ1	Wat23	Asn93 Nδ2
Wat15	Wat23	Lys96 Nζ
V_L Trp94 N	Wat51	Arg21 Nϵ
	Wat51	Wat50
V_L Ser30 Oγ	Wat58	Lys13 O
Wat257	Wat58	Asp18 N
V_L Tyr50 Oη	Wat79	Asn93 O
	Wat79	Wat284
V_H Tyr58 Oη	Wat121	Val99 O
Wat405	Wat121	Asp101 O
V_L Ser67 Oγ	Wat174	Arg14 O
	Wat174	Wat40
V_L Ser28 O	Wat359	Asn19 Nδ2
	Wat359	Wat270
V_L Ser67 Oγ	Wat418	Lys13 O

[a] Water molecules in the interface.

Table 5: Root-Mean-Square Differences after Superpositions of HyHEL-63 and HyHEL-10 V and C Domains[a]

domain	P11-P12	C2-P11	C2-P12	C2-H63−HEL	P11-H63−HEL	P12-H63−HEL	H63−HEL-H10−HEL
Fab−HEL	−	−	−	−	−	−	4.00 (3.08)
Fab	1.00 (0.86)	1.05 (1.04)	0.91 (0.80)	0.86 (0.65)	0.95 (0.76)	0.79 (0.67)	3.73 (2.93)
Fv	0.50 (0.24)	0.49 (0.40)	0.51 (0.39)	0.60 (0.42)	0.62 (0.37)	0.52 (0.37)	0.91 (0.68)
V_L	0.30 (0.21)	0.38 (0.31)	0.33 (0.31)	0.44 (0.44)	0.34 (0.27)	0.37 (0.26)	0.91 (0.55)
V_H	0.58 (0.30)	0.49 (0.37)	0.42 (0.27)	0.54 (0.33)	0.73 (0.37)	0.54 (0.31)	0.77 (0.62)
C_H1 and C_L	0.76 (0.31)	0.53 (0.40)	0.70 (0.24)	0.88 (0.39)	0.88 (0.46)	0.70 (0.41)	1.59 (0.69)
C_L	0.61 (0.27)	0.52 (0.24)	0.66 (0.21)	0.63 (0.34)	0.37 (0.24)	0.60 (0.38)	1.10 (0.55)
C_H1	0.83 (0.30)	0.40 (0.35)	0.71 (0.18)	1.02 (0.30)	1.12 (0.40)	0.71 (0.31)	1.76 (0.76)

[a] Fab, HyHEL-63; P11, Fab1 in the *P*1 space group; P12, Fab2 in the *P*1 space group; C2, Fab in the *C*2 space group; H63−HEL, HyHEL-63−HEL complex; H10−HEL, HyHEL-10−HEL complex; and Fab−HEL, Fab−HEL complex. Numbers in parentheses show the rms deviations after 3σ outliers were removed from the comparisons.

(Wat121) is found to hydrogen bond with a V_H residue (Tyr58); all the others interact with V_L residues.

The structure of the Fab HyHEL-63−HEL complex illustrates the importance of bound water molecules in mediating antigen−antibody interactions. Indeed, with only one exception (*15*), water molecules have been localized in the interfaces of each of the antigen−antibody complexes whose crystal structures have been determined at sufficiently high resolution (<2.5 Å) to allow the identification of ordered waters with a reasonable degree of accuracy (*10*, *11*, *19*, *20*). It therefore appears that water molecules are required to correct imperfections in antigen−antibody interfaces by improving the fit between the proteins and by neutralizing unpaired hydrogen-bonding groups. Bound waters, acting as molecular adaptors, may compensate for the lack of evolutionary optimization of antigen−antibody interfaces, compared to other protein−protein interfaces in which the interacting surfaces may have coevolved to maximize complementarity (e.g., oligomeric proteins).

Conformational Differences between Free and Bound HyHEL-63 and HEL. The availability of high-resolution crystal structures for free HEL in three crystal forms (*48*−*50*) and for free Fab HyHEL-63 in two crystal forms (*P*1 and *C*2) allows us to assess whether any conformational changes occur in the antigen or antibody upon complex formation. In addition, because the *P*1 form of HyHEL-63 contains two copies of the Fab per asymmetric unit (designated H63-P1 molecules 1 and 2), we in effect know the structure of the free antibody in three different crystal packing environments.

As show in Table 5, the structural comparison between free and bound HyHEL-63 was carried out at three levels: (1) superposition of entire Fabs, (2) superposition of V (V_L and V_H) and C (C_L and C_H1) modules, and (3) superposition of individual V_L, V_H, C_L, or C_H1 domains. In general, the root-mean-square (rms) deviations in α-carbon positions for the fit of individual domains are lower than those for the fit of whole Fabs. The V_L domain shows consistently low rms deviations between the free and bound Fabs, or between the free Fab in different crystal forms. This is also true for the C_L domain of HyHEL-63. For the V_H and C_H domains, however, the rms differences are generally greater and more variable. The rms deviations between the free and complexed Fabs also include differences in V_L-V_H domain association. For example, the best fit of antigen-bound V_H onto free V_H in H63-C2 is achieved by a 1.7° rotation relative to the best fit of V_L domains. However, this difference may be related only partially, or not at all, to antigen binding. When the V_L domains of the free Fabs are optimally superposed, a 1.1° rotation is needed to obtain the best fit for the V_H domains of the two copies of the free Fab in the asymmetric unit in H63-P1. In addition, a 2.4° rotation is required to best superpose the V_H domain of the free Fab in the H63-C2 structure onto that of H63-P1 molecule 1, following the superposition of the V_L domains. Nevertheless, it can be argued that HEL binding, which buries nearly 2000 Å^2 of the surface in the complex, should have at least as much influence on V_L-V_H domain association as less extensive crystal packing interactions. The observed differences in domain association affect the interdomain hydrogen bonding network of the V_L-V_H dimers (Table 6). Five out of 8 pairs of the hydrogen bonds between the V_L and V_H domains of HyHEL-63 are not conserved upon complex formation, or in different crystal forms, whereas 2 hydrogen bonds between V_L Ser43 Oγ and V_H Gly104 O and between V_L Trp94 Nϵ1 and V_H Tyr59 O are preserved in all four Fab structures (H63-P1 molecules 1 and 2, H63-C2, and complexed Fab). In addition, the hydrogen bond between the hydroxy group of V_H Tyr94 and V_L Gln38 is conserved, although in H63-C2, the V_H Tyr94 hydroxy group hydrogen bonds to Oϵ1 of V_L Gln38, instead of to Nϵ2 as in the other three cases (Table 6). The relative orientation of V and C modules in bound versus free Fab HyHEL-63 in space group *C*2 appears unchanged upon complex formation, as reflected by an elbow angle of 187° for both structures. However, when viewed in three dimensions following optimal superposition of V_L and V_H, the C modules of the two Fabs require a 3.8° rotation to achieve the best fit. This difference is probably attributable to flexibility at the elbow region, rather than to antigen binding, as noted for other Fab−HEL complexes (*2*−*6*).

Table 6: Hydrogen Bonds between V_L and V_H in Free and HEL-Bound HyHEL-63[a]

	V_H pairs			
V_L residues	H63-C2	H63-P11	H63-P12	H63−HEL
Tyr36 Oη	−	Asp99 O	Asp99 O	−
Gln38 Oϵ1	Lys39 Nζ	−	−	Lys39 Nζ
Oϵ1	Tyr94 Oη	−	−	−
Gln38 Nϵ2	−	Tyr94 Oη	Tyr94 Oη	Tyr94 Oη
Ser43 Oγ	Gly104 O	Gly104 O	Gly104 O	Gly104 O
Oγ	Ala105 O	−	−	−
Trp94 Nϵ1	Tyr59 O	Tyr59 O	Tyr59 O	Tyr59 O
Tyr96 Oη	−	−	−	Trp98 Nϵ1

[a] C2-H63 refers to free Fab HyHEL-63 in the *C*2 space group. H63-P11 and H63-P12 refer to free Fab molecules 1 and 2, respectively, in the *P*1 space group.

Table 7 lists those regions of HyHEL-63 V_L-V_H with rms deviations in α-carbon positions greater than 1.0 Å following

Table 7: Regions with Different Conformations between Free and Complexed Fab HyHEL-63 or between Different Crystal Forms of the Free Fab[a]

region	P11-P12	C2-P11	C2-P12	C2-H63−HEL	P11-H63−HEL	P12-H63−HEL	H63−HEL-H10−HEL
V_L	−	−	−	−	−	−	14−18
V_L	−	40	40	−	40 and 41	−	−
V_L	−	−	−	−	−	−	39−41
V_L	−	−	−	56 and 57	56 and 57	56 and 57	−
V_L	−	−	−	−	−	−	58−63
V_L	−	−	−	94	−	−	−
V_L	108 and 109	109	−	109	−	108 and 109	105−109
V_H	1	−	−	−	1	−	1 and 2
V_H	−	−	−	−	−	−	12
V_H	−	−	−	−	−	−	18
V_H	15 and 16	15 and 16	−	−	15 and 16	−	−
V_H	26 and 27	−	31	−	−	−	25−31
V_H	−	−	−	41−43	41−43	41−43	−
V_H	53−55	−	53−55	53−56	53−56	53 and 54	−
V_H	64	−	64	63 and 64	64	64	64
V_H	−	−	−	99	98 and 99	98 and 99	98 and 99
V_H	113	−	112 and 113	−	−	−	113

[a] Fab, HyHEL-63; P11, Fab1 in the *P*1 space group; P12, Fab2 in the *P*1 space group; C2, Fab in the *C*2 space group; H63−HEL, HyHEL-63−HEL complex; H10−HEL, HyHEL-10−HEL complex; and Fab−HEL, Fab−HEL complex. Regions listed are those with rms deviations in α-carbon positions of >1.0 Å.

superposition of individual V_L and V_H domains in free and complexed forms of the antibody. The differences arise from four sources: (1) flexibility in the N- or C-termini; (2) flexibility in loop regions, including CDRs; (3) crystallographic contacts; and (4) antigen binding. The first three categories reflect local flexibilities in the antibody structures. Thus, conformational differences in residues V_L 108 and 109, V_H 1, and V_H 112 and 113 fall into category 1. Residues V_L 40 and 41 and V_H 41−43 are located in loops forming part of the interface of the V_L−V_H dimer and belong to category 2. The structural differences in these loops are only observed between the free and complexed Fabs, indicating that the changes could be attributable to antigen binding. Similarly, differences in residues V_L 56 and 57 are only observed between the complexed and free Fab structures, even though these residues do not directly contact HEL. However, in this case, the differences probably result from different crystallographic contacts, rather than from antigen binding since, in all free Fab forms, residues V_L 56 and 57 make no contacts with symmetry-related molecules, whereas in the HyHEL-63−HEL complex, they form three hydrogen bonds with symmetry mates. Conformational differences in residues V_H 15 and 16 also probably arise from different crystallographic contacts.

As shown in Table 7, significant differences in HyHEL-63 residues V_H 98 and 99, located at the tip of V_H CDR3, are only observed between the complexed and free Fabs, not between the free Fabs in different crystal forms, or between H63-P1 molecules 1 and 2. In antibody molecules, V_H CDR3 generally comprises a major portion of the combining site and is located near its geometrical center. Thus, conformational changes in this region are likely to be related to antigen binding. Compared with its position in the free Fab structures, the V_H CDR3 loop in the complexed Fab is pushed back by up to 1.9 Å in the position of the Gly99 α-carbon atom (Figure 6A). This displacement appears necessary to avoid steric clashes between the antigen and antibody in the complex. Significant differences are also found in the relative position of V_H CDR2 residues 53−56. A displacement of 2.7 Å occurs in the position of the Ser54 α-carbon atom in the HyHEL-63−HEL complex compared

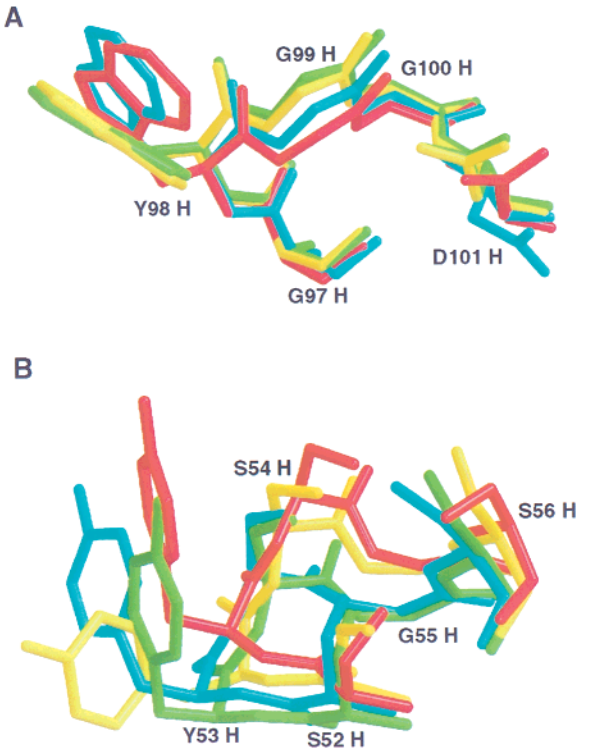

FIGURE 6: (A) Conformational differences in V_H CDR3. Complexed Fab HyHEL-63 (red) was superposed onto three different forms of the free antibody (H63-C2, blue; H63-P1 molecule 1, green; and H63-P2 molecule 2, yellow). (B) Conformational differences in V_H CDR2. Bound and unbound Fab HyHEL-63 are colored as in panel A.

with its position in free H63-P1 molecule 1 (Figure 6B); similar displacements are observed in comparisons with the other free Fab structures. Furthermore, the changes are significantly greater than between the free Fabs in different crystal forms, suggesting that they result from the binding of HEL. As shown in Table 2, V_H residues Tyr53, Ser54, and Ser56 make a total of 6 hydrogen bonds with HEL. Compared to the free Fab structures, the peptide backbone of these residues appears to be lifted toward the antigen to maximize productive interactions between HyHEL-63 and

HEL. In addition to concerted movements of the peptide backbone, changes in the orientations of several side chains also occur upon complex formation. For instance, in the free Fab structures, the side chain of V_H Ser56 has nearly the same orientation, while in the complex, the side chain rotates about 100° to make hydrogen bonds with HEL residues Asp101 and Gly102 (Figure 6B).

The conformational differences described above between free and HEL-bound Fab HyHEL-63 are similar in magnitude to those observed in the four other complexes involving protein antigens for which the structure of the antibody in both free and antigen-bound forms is known: Fv D1.3−HEL (*20*), Fab D44.1−HEL (*6*), Fab E8−cytochrome *c* (*10*), and Fab 5G9−tissue factor (*11*). In all five cases, structural rearrangements in the antibody upon antigen binding are restricted to (1) small (<3 Å) concerted movements in the CDR loops, (2) side chain rearrangements, and (3) slight shifts in the relative orientation of the V_L and V_H domains, equivalent to rotations of <3°. Somewhat larger conformational changes, including CDR loop displacements of up to 5 Å, have been described for certain complexes involving DNA or peptide antigens (*51*).

In the structure determination of the Fab HyHEL-63−HEL complex (see Experimental Procedures), the starting search model for HEL was taken from the Fv D1.3−HEL complex (*23*). However, the final model of HEL in the HyHEL-63−HEL complex differs from that of HEL complexed with D1.3 for loop residues 99−104, with a displacement of 6.8 Å in the position of the Gly102 α-carbon atom. The loop of residues 99−104 comprises part of the epitope recognized by HyHEL-63, contributing 8 hydrogen bonds between HEL residues Asp101, Gly102, and Asn103 and V_H CDR2 residues Ser52, Tyr53, Ser54, Ser56, and Tyr58 (Table 2). Residues 102 and 103 are also part of the epitope recognized by D1.3, forming one direct hydrogen bond between HEL Gly102 O and V_H Arg98 Nη1 and one water-mediated hydrogen bond between Asp103 Oδ1 and V_H Arg98 Nη2 (*23*). Therefore, the epitopes of HEL recognized by antibodies D1.3 and HyHEL-63 partially overlap, which may explain the large difference in the main chain conformations of residues 99−104 in the two complexes. A comparison of bound HEL in the HyHEL-63−HEL complex with free HEL in two crystal forms (tetragonal and monoclinic) (*48*, *49*) reveals that the main chain conformation of HEL residues 101−103 in the complex is very similar to that in the two free forms. A displacement of 1.3 Å in the position of the Gly102 α-carbon atom is observed, not nearly as large as the 6.8 Å difference noted above in a comparison of the D1.3−HEL and HyHEL-63−HEL structures. In the tetragonal form of free HEL (*50*), the loop of residues 99−104 adopts yet another main chain conformation, different from those discussed above, indicating flexibility. In addition, the loop has undergone a peptide flip between residues Asp101 and Gly102 in the complex compared to its structure in the free forms. This backbone conformational change results in a displacement of the Asp101 side chain, permitting it to form 5 hydrogen bonds with V_H CDR2 (Asp101 Oδ1−V_H Ser52 Oγ, Asp101 Oδ1−V_H Ser54 N, Asp101 Oδ1−V_H Ser54 Oγ, Asp101 Oδ2−V_H Ser54 Oγ, and Asp101 Oδ1−V_H Ser56 Oγ), presumably enhancing complex stability.

Antigen-bound Fab HyHEL-63 exhibits reduced temperature factors (*B*) compared with the free antibody (not shown), suggesting that conformational entropy decreases upon complex formation. In fact, the entire HyHEL-63 L chain (both V_L and C_L domains) is generally less mobile in the complex, as reflected by an average *B* value of 21 Å^2, than in the free Fab structures (*B* values of 27 and 29 Å^2 for H63-P1 molecules 1 and 2, respectively, and 30 Å^2 for H63-C2). An overall decrease in mobility of a whole antibody domain (V_H) was also observed in the Fab D44.1−HEL complex (*6*), but this reduction did not extend to the entire D44.1 H or L chain. The V_H CDR1 and CDR2 loops of HyHEL-63 exhibit similar thermal values in the bound and free antibodies, while the mobility of V_H CDR3 is markedly reduced in the complex, in agreement with the fact that this loop is located in the center of the antibody-combining site.

Comparison with the HyHEL-10−HEL Complex. The overall rms deviation between the HyHEL-10−HEL and HyHEL-63−HEL complexes is 4.00 Å (Table 5). However, this is mostly attributable to differences in the C_H1 domains of the Fab fragments: HyHEL-10 and HyHEL-63 are IgG1 and IgG2a antibodies, respectively. If only the HEL and V_L and V_H portions of the complexes are compared, the rms deviation is 0.85 Å. The solvent-excluded surface area for the HyHEL-10−HEL complex is 1787 Å^2 (859 Å^2 from HyHEL-10 and 928 Å^2 from HEL). This buried surface is 114 Å^2 smaller than for the HyHEL-63−HEL complex (1901 Å^2), which is almost equally contributed by HyHEL-63 and HEL (Table 3). Thus, the HEL epitope recognized by HyHEL-63 is slightly larger than that recognized by HyHEL-10.

The V_L sequences of HyHEL-63 and HyHEL-10 differ at 2 positions (17 and 30) and the V_H sequences at 10 (1, 29, 44, 51, 81, 97, 99, 102, 105, and 108) (Figure 1). Of these differences, 1 is in V_L CDR1 (V_L 30), 1 is in V_H CDR2 (V_H 51), and 2 are in V_H CDR3 (99 and 102). However, only residue V_L 30 (Ser in HyHEL-63 and Gly in HyHEL-10) makes contacts with HEL in both complexes; residue V_H 102 (Val in HyHEL-63 and Tyr in HyHEL-10) contacts the antigen only in the HyHEL-10−HEL complex, contributing 7 Å^2 to the buried surface area. In the HyHEL-63−HEL complex, V_L Ser30 makes 3 van der Waals contacts with HEL, compared to 5 made by V_L Gly30 in the HyHEL-10−HEL complex. Although the contacting residues are nearly identical in the two complexes, there are 24 hydrogen bonds in the HyHEL-63−HEL interface, but only 20 in the HyHEL-10−HEL interface (Table 2). Surprisingly, only 12 of these hydrogen bonds are conserved in the two structures.

Since the resolution of the HyHEL-10−HEL complex (3 Å) is insufficient to reveal ordered water molecules, the solvent structure in the HyHEL-63−HEL and HyHEL-10−HEL interfaces cannot be compared. However, it is very likely that bound waters are also present in the HyHEL-10−HEL complex, bridging the antigen and antibody.

A peptide flip is observed between V_L CDR1 residues 30 and 31 in the HyHEL-10−HEL and HyHEL-63−HEL complexes, probably caused by the Gly → Ser30 substitution in HyHEL-63. A peptide flip is also found between V_H CDR2 residues 53 and 54. Significant main chain conformational differences occur at V_H positions 25−31 (FR1 and CDR1) and 98 and 99 (CDR3) (Table 7), which may result from the Val29 → Ile substitution in HyHEL-10. The hydrophobic side chain of V_H residue 29 normally intercalates between two β-pleated sheets, thereby stabilizing the conformation

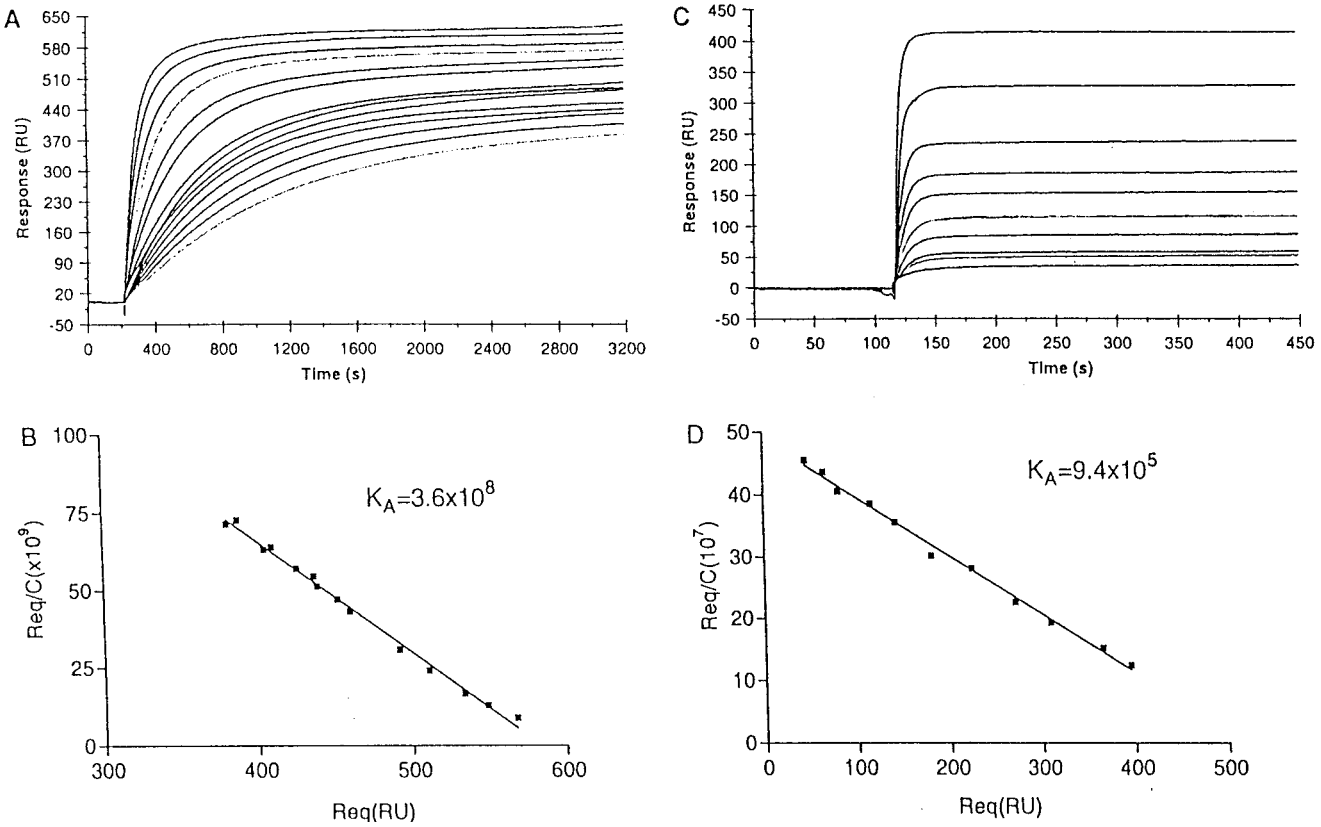

FIGURE 7: (A) Binding of Fab HyHEL-63 to immobilized wild-type HEL. Fab HyHEL-63 was injected at 14 different concentrations ranging from 5.3 to 64 nM over a surface to which 550 RU of wild-type HEL had been coupled. Buffer flow rates were 5 μL/min. Equilibrium binding levels were reached within 50 min. After equilibrium had been reached, residual bound protein was eluted using a 1 min pulse of 10 mM HCl. (B) Scatchard plot of the binding of Fab HyHEL-63 to wild-type HEL derived from the data depicted in panel A after correction for nonspecific binding; R_{eq} is the corrected equilibrium response at a given concentration C. The plot is linear with a correlation coefficient of 0.99. The apparent K_A is 3.6×10^8 M^{-1}. The predicted maximum binding capacity (1900 RU) indicates that about 30% of the immobilized wild-type HEL molecules are available for binding. (C) Binding of Fab HyHEL-63 to the immobilized HEL K97A mutant. Fab HyHEL-63 was injected at 10 different concentrations ranging from 0.1 to 3.2 μM over a surface to which 420 RU of HEL K97A had been coupled. (D) Scatchard plot derived from the data depicted in panel C after correction for nonspecific binding. The plot is linear with a correlation coefficient of 0.99, and the apparent K_A is 9.4×10^5 M^{-1}. Approximately 35% of the immobilized HEL K97A is available for binding as calculated from the predicted maximum binding capacity (1500 RU).

of the V_H CDR1 loop. The rms deviation between the α-carbon positions of V_H residue 29 in the two complexes is 1.51 Å, equal to a carbon−carbon bond length and consistent with isoleucine having 1 more carbon atom than valine. Differences are also observed in the V_H CDR3 loop conformation, which may be a consequence of the Gly99 → Asp substitution in HyHEL-10. In the HyHEL-10−HEL complex, the side chain of V_H Asp99 has the potential to hydrogen bond with V_L residues His34 and Lys49, whereas in the HyHEL-63−HEL complex, V_H Gly99 O is linked to V_L Lys49 Nζ via a water-mediated hydrogen bond. This difference apparently alters the side chain conformation of V_H Trp98, a crucial residue for HEL binding.

In the HEL portion of the HyHEL-63−HEL and HyHEL-10−HEL complexes, a 110° rotation is observed for the side chain of Trp62. However, this residue is only partially buried in the complexes (<30%) and makes few contacts with the Fabs. Furthermore, its side chain conformation varies significantly in the free HEL structures (*48*−*50*). In contrast, HEL Lys97, which also displays very different side chain conformations in the free HEL structures (*48*−*50*), has very similar conformations in the HyHEL-63−HEL and HyHEL-10−HEL complexes, which differ from those in the free antigen structures. The conformation of HEL Lys97 in the complexes is likely to be restricted by the bulky side chains of V_H residues Tyr33 and Trp98, as well as by the salt bridge to V_H Asp32 (Table 2).

Affinity of the HyHEL-63−HEL Interaction and Effects of Mutations in HEL on Binding. A surface plasmon resonance profile for equilibrium binding of Fab HyHEL-63 to immobilized wild-type HEL is shown in Figure 7A. The corresponding Scatchard plot, after correction for nonspecific binding, is also shown (Figure 7B). The apparent K_A (3.5×10^8 M^{-1}) was calculated as the slope of the straight line. This compares with a K_A of 7.7×10^9 M^{-1} for the Fab HyHEL-10−HEL interaction (*52*), indicating that HyHEL-63 binds approximately 20-fold less tightly to HEL than HyHEL-10. This relatively small affinity decrease could be due to amino acid differences at two antigen-contacting positions, V_L 30 and V_H 102, and/or to differences in noncontacting positions, such as V_H 99, that may subtly alter the conformation or mobility of CDR loops in contact with HEL.

To assess the relative contribution of selected HEL residues to the stabilization of the HyHEL-63−HEL complex, alanine-scanning mutagenesis was carried out on 5 antigen residues in contact with the antibody in the crystal structure. Figure 7C shows a BIAcore profile for equilibrium

Table 8: Association Constants and Relative Free Energy Changes for the Binding of HEL Mutants to HyHEL-63

HEL	K_A (M^{-1})	$\Delta\Delta G$ (kcal/mol)
wild type	$(3.6 \pm 0.1) \times 10^8$	
Y20A	$(1.4 \pm 0.1) \times 10^6$	3.4
R21A	$(5.0 \pm 0.2) \times 10^7$	1.2
W63A	$(3.7 \pm 0.1) \times 10^7$	1.4
K97A	$(9.4 \pm 0.2) \times 10^5$	3.6
D101A	$(3.1 \pm 0.1) \times 10^7$	1.5

binding of Fab HyHEL-63 to the immobilized HEL K97A mutant. Scatchard analysis (Figure 7D) yields an apparent K_A of 9.4×10^5 M^{-1}, 370-fold less than that for wild-type HEL, which corresponds to a relative loss in binding free energy ($\Delta G_{mutant} - \Delta G_{wild\ type}$) of 3.6 kcal/mol (Table 8). A comparable reduction in the binding energy ($\Delta\Delta G = 3.4$ kcal/mol) was observed for the HEL Y20A mutant, whereas alanine substitutions at HEL positions 21, 63, and 101 had less pronounced effects (1.2−1.5 kcal/mol). These results may be readily understood in terms of the three-dimensional structure of the HyHEL-63−HEL complex. Thus, HEL residues Lys97 and Tyr20 are located at the center of the interface and are completely (Tyr20), or almost completely (Lys97), buried upon complex formation. In addition, the side chain nitrogen of HEL Lys97 forms a salt bridge with the side chain carboxylate moiety of V_H Asp32, while the HEL Tyr20 hydroxy group hydrogen bonds with the amide nitrogen of V_L Gln53 (Table 2). In contrast, HEL residues Arg21, Trp63, and Asp101 are located at the periphery of the interface and are only partially buried in the complex. Although HEL Arg21 and Arg101 form a number of hydrogen bonds with HyHEL-63 residues, these are solvent-exposed. Double mutant cycle analysis of solvated hydrogen bonds in the D1.3−HEL interface has clearly demonstrated that they make little or no net contribution to complex stabilization (*23*). Furthermore, X-ray crystallographic studies of mutant D1.3−HEL complexes have shown that alanine substitutions at solvent-accessible sites are compensated by the stable incorporation of additional water molecules in the interface and by local solvent rearrangements that help fill cavities created by side chain truncations and preserve the hydrogen bonding network linking the antigen and antibody (*22*, *23*). Similar mechanisms are likely to explain the relatively greater tolerance of the HyHEL-63−HEL interface to mutations in HEL residues 21, 63, and 101, which are mostly solvent-exposed in the complex, than to mutations in residues 20 and 97, which are mostly buried. Thus, the HyHEL-63-combining site appears to comprise a cluster of hot spot residues at the center surrounded by energetically less important residues that serve to largely exclude bulk solvent from the hot spots, in common with other protein−protein complexes (*1*, *58*).

Conclusions. We have determined the crystal structures of free and HEL-bound HyHEL-63 to high resolution. In the complex, the contacting surface of the antibody is mainly hydrophobic, whereas hydrophilic residues predominate on the HEL side of the interface. The structures reveal that complementarity between the interacting surfaces is enhanced by small, but significant, movements in the polypeptide backbones of both the antigen and antibody and by rearrangements of interface side chains. Complementarity is further enhanced by a number of interface water molecules, several of which are completely buried in the complex. Water molecules have also been localized in the interfaces of certain other protein−protein complexes whose structures have been determined to high resolution, including protease−protease inhibitor complexes (*53*, *54*), a barnase−barstar complex (*55*), the complex of vascular endothelial growth factor with its receptor (*56*), and the growth hormone−growth hormone receptor complex (*57*). In each case, bound waters contribute to complex stability by neutralizing unpaired hydrogen-bonding groups and by improving the fit between the proteins. Therefore, water-mediated contacts are not restricted to antigen−antibody complexes and are probably characteristic of many protein−protein interfaces.

The HyHEL-63−HEL complex constitutes an excellent model for detailed structure−function studies of protein−protein recognition by alanine-scanning mutagenesis, double mutant cycles, and X-ray crystallography. Not only are the crystal structures of both free and bound HyHEL-63 and HEL known to high resolution, but mutants of the antibody and antigen can be readily produced in bacteria and yeast, respectively. Furthermore, the affinities of mutant complexes can be accurately measured under equilibrium binding conditions using surface plasmon resonance methods. Thus, it should be possible to interpret the results of single and double mutant cycle experiments in the Fab HyHEL-63−HEL system in terms of the three-dimensional structures of the corresponding mutant complexes, as in the Fv D1.3−HEL system (*21*−*23*). A comparison of the results obtained from these two independent models should significantly advance our understanding of how structural features of protein−protein interfaces contribute to the affinity and specificity of macromolecular association reactions.

REFERENCES

1. Lo Conte, L., Chothia, C., and Janin, J. (1999) *J. Mol. Biol. 285*, 2177−2198.
2. Amit, A. G., Mariuzza, R. A., Phillips, S. E. V., and Poljak, R. J. (1986) *Science 233*, 747−753.
3. Sheriff, S., Silverton, E. W., Padlan, E. A., Cohen, G. H., Smith-Gill, S. J., Finzel, B. C., and Davies, D. R. (1987) *Proc. Natl. Acad. Sci. U.S.A. 84*, 8075−8079.
4. Padlan, E. A., Silverton, E. W., Sheriff, S., Cohen, G. H., Smith-Gill, S. J., and Davies, D. R. (1989) *Proc. Natl. Acad. Sci. U.S.A. 86*, 5938−5942.
5. Chitarra, V., Alzari, P. M., Bhat, T., Eiselé, J.-L., Houdusse, A., Lescar, J., Souchon, H., and Poljak, R. J. (1993) *Proc. Natl. Acad. Sci. U.S.A. 90*, 7711−7715.
6. Braden, B. C., Souchon, H., Eiselé, J.-L., Bentley, G. A., Bhat, T. N., Navaza, J., and Poljak, R. J. (1994) *J. Mol. Biol. 243*, 767−780.
7. Colman, P. M., Laver, W. G., Varghese, J. N., Baker, A. T., Tulloch, P. A., Air, G. M., and Webster, R. G. (1987) *Nature 326*, 358−363.
8. Tulip, W. R., Varghese, J. N., Laver, W. G., Webster, R. G., and Colman, P. M. (1992) *J. Mol. Biol. 227*, 122−148.
9. Malby, R. L., Tulip, W. R., Harley, V. R., McKimm-Breschkin, J. L., Laver, W. G., Webster, R. G., and Colman, P. M. (1994) *Structure 2*, 733−746.
10. Mylvaganam, S. E., Paterson, Y., and Getzoff, E. D. (1998) *J. Mol. Biol. 281*, 301−322.
11. Huang, M., Syd, R., Stura, E. A., Stone, M. J., Stefanko, R. S., Ruf, W., Edgington, T. S., and Wilson, I. A. (1998) *J. Mol. Biol. 275*, 873−894.
12. Prasad, L., Sharma, S., Vandonselaar, M., Quail, J. W., Lee, J. S., Waygood, B., Wilson, K. S., Dauter, Z., and Delbaere, T. J. (1993) *J. Biol. Chem. 268*, 10705−10708.

13. Bossart-Whitaker, P., Chang, C. Y., Novotny, J., Benjamin, D. C., and Sheriff, S. (1995) *J. Mol. Biol. 253*, 559−575.
14. Bizebard, T., Gigant, B., Rigolet, P., Rasmussen, B., Diat, O., Bosecke, P., Wharton, S. A., Skehel, J. J., and Knossow, M. (1995) *Nature 376*, 92−94.
15. Muller, Y. A., Chen, Y., Christinger, H. W., Li, B., Cunningham, B. C., Lowman, H. B., and de Vos, A. M. (1998) *Structure 6*, 1153−1167.
16. Bentley, G. A., Boulot, G., Riottot, M. M., and Poljak, R. J. (1990) *Nature 348*, 254−257.
17. Ban, N., Escobar, C., Garcia, R., Hasel, K., Day, J., Greenwood, A., and McPherson, A. (1994) *Proc. Natl. Acad. Sci. U.S.A. 91*, 1604−1608.
18. Evans, S. V., Rose, D. R., To, R., Young, N. M., and Bundle, D. (1994) *J. Mol. Biol. 241*, 691−705.
19. Fields, B. A., Goldbaum, F. A., Ysern, X., Poljak, R. J., and Mariuzza, R. A. (1995) *Nature 374*, 739−742.
20. Bhat, T. N., Bentley, G. A., Boulot, G., Greene, M. I., Tello, D., Dall'Acqua, W., Souchon, H., Schwarz, F. P., Mariuzza, R. A., and Poljak, R. J. (1994) *Proc. Natl. Acad. Sci. U.S.A. 91*, 1089−1093.
21. Dall'Acqua, W., Goldman, E. R., Eisenstein, E., and Mariuzza, R. A. (1996) *Biochemistry 35*, 9667−9676.
22. Fields, B. A., Goldbaum, F. A., Dall'Acqua, W., Malchiodi, E. L., Cauerhff, A., Schwarz, F. P., Ysern, X., Poljak, R. J., and Mariuzza, R. A. (1996) *Biochemistry 35*, 15494−15503.
23. Dall'Acqua, W., Goldman, E. R., Lin, W., Teng, C., Tsuchiya, D., Li, H., Ysern, X., Braden, B. C., Li, Y., Smith-Gill, S. J., and Mariuzza, R. A. (1998) *Biochemistry 37*, 7981−7991.
24. Clackson, T., and Wells, J. A. (1995) *Science 267*, 383−386.
25. Goldman, E. R., Dall'Acqua, W., Braden, B. C., and Mariuzza, R. A. (1997) *Biochemistry 36*, 49−56.
26. Schreiber, G., and Fersht, A. R. (1995) *J. Mol. Biol. 248*, 478−486.
27. Newman, M. A., Mainhart, C. R., Mallett, C. P., Lavoie, T. B., and Smith-Gill, S. J. (1992) *J. Immunol. 149*, 3260−3272.
28. Smith-Gill, S. J., Mainhart, C., Lavoie, T. B., Feldman, R. J., Drohan, W., and Brooks, B. R. (1987) *J. Mol. Biol. 194*, 713−724.
29. Jancarik, J., and Kim, S.-H. (1991) *J. Appl. Crystallogr. 24*, 409−411.
30. Otwinowski, Z., and Minor, W. (1997) *Methods Enzymol. 276*, 307−326.
31. Collaborative Computational Project No. 4 (1994) *Acta Crystallogr. D50*, 760−763.
32. Navaza, J. (1994) *Acta Crystallogr. A50*, 157−163.
33. Smith, T. F., and Waterman, M. (1981) *J. Mol. Biol. 147*, 195−197.
34. Celikel, R., Williamson, M. M., Ni, C.-Z., and Ely, K. R. (1993) *Acta Crystallogr. D49*, 421−422.
35. Li, H., Dunn, J. J., Luft, B. J., and Lawson, C. L. (1997) *Proc. Natl. Acad. Sci. U.S.A. 94*, 3584−3588.
36. Charbonnier, J.-B., Golinelli-Pimpaneau, B., Gigant, B., Tawfik, D. S., Chap, R., Schindler, D. G., Kim, S.-H., Green, B. S., Eshar, Z., and Knossow, M. (1997) *Science 275*, 1140−1142.
37. Brunger, A. T. (1992) *X-PLOR Version 3.1. A System for X-ray Crystallography and NMR*, Yale University Press, New Haven, CT.
38. Brunger, A. T., Adams, P. D., Clore, G. M., DeLano, W. L., Gros, P., Grosse-Kunstleve, R. W., Jiang, J.-S., Kuszewski, J., Nilges, M., Pannu, N. S., Read, R. J., Rice, L. M., Simonson, T., and Warren, G. L. (1998) *Acta Crystallogr. D54*, 905−921.
39. Roussel, A., and Cambillau, C. (1989) TURBO-FRODO, in *Silicon Graphics Geometry Partners Directory*, pp 77−78, Silicon Graphics, Mountain View, CA.
40. Lee, B., and Richards, F. M. (1971) *J. Mol. Biol. 55*, 379−400.
41. Satow, Y., Cohen, G. H., Padlan, E. A., and Davies, D. R. (1986) *J. Mol. Biol. 190*, 593−604.
42. Kunkel, T. A., Roberts, J. D., and Zakour, R. A. (1987) *Methods Enzymol. 154*, 367−382.
43. Li, Y., Grivel, J.-C., Visiwanathan, M., Srinivasan, M., and Smith-Gill, S. J. (1997) *FASEB J. 11*, A1043.
44. Malcolm, B. A., Rosenberg, S., Corey, M. J., Allen, J. S., de Baetselier, A., and Kirsch, J. F. (1989) *Proc. Natl. Acad. Sci. U.S.A. 86*, 133−137.
45. Kodandapani, R., Veerapandian, B., Kunicki, T. J., and Ely, K. R. (1995) *J. Biol. Chem. 270*, 2268−2273.
46. Luzzatti, V. (1952) *Acta Crystallogr. A5*, 802−810.
47. Lawrence, M. C., and Colman, P. M. (1993) *J. Mol. Biol. 234*, 946−950.
48. Ramanadham, M., Sieker, L. C., and Jensen, L. H. (1990) *Acta Crystallogr. B46*, 63−69.
49. Wilson, K. P., Malcolm, B. A., and Matthews, B. W. (1992) *J. Biol. Chem. 267*, 10842−10849.
50. Madhusudan, Kodandapani, R., and Vijayan, M. (1993) *Acta Crystallogr. D49*, 234−245.
51. Wilson, I. A., and Stanfield, R. L. (1993) *Curr. Opin. Struct. Biol. 3*, 113−118.
52. Kam-Morgan, L. N. W., Smith-Gill, S. J., Taylor, M. G., Zhang, L., Wilson, A. C., and Kirsch, J. F. (1993) *Proc. Natl. Acad. Sci. U.S.A. 90*, 3958−3962.
53. Bolognesi, M., Gatti, G., Menegatti, E., Guarneri, M., Marquart, M., Papamokos, E., and Huber, R. (1982) *J. Mol. Biol. 162*, 839−868.
54. McPhalen, C. A., and James, M. N. G. (1988) *Biochemistry 27*, 6582−6598.
55. Buckle, A., Schreiber, G., and Fersht, A. R. (1994) *Biochemistry 33*, 8878−8889.
56. Weismann, C., Fu, G., Christinger, H. W., Eigenbrot, C., Wells, J. A., and De Vos, A. M. (1997) *Cell 91*, 695−704.
57. Clackson, T., Ultsch, M. H., Wells, J. A., and De Vos, A. M. (1998) *J. Mol. Biol. 277*, 1111−1128.
58. Bogan, A. A., and Thorn, K. S. (1998) *J. Mol. Biol. 280*, 1−9.
59. Kabat, E. A., Wu, T. T., Perry, H. M., Gottesman, K. S., and Foeller, C. (1991) *Sequences of Proteins of Immunological Interest*, 5th ed., Public Health Services, National Institutes of Health, Washington, DC.
60. Nicholls, A., Bharadwaj, R., and Honig, B. (1993) *Biophys. J. 64*, 166.

BI000054L